International Journal of Mechanical Sciences 277 (2024) 109391

Contents lists available at ScienceDirect

International Journal of Mechanical Sciences

journal homepage: www.elsevier.com/locate/ijmecsci

A continuum model for granular materials exhibiting a smooth transition between inelastic flow and elastic jamming

M.B. Rubin [a,1], J. Ciambella [b,*,1], B. Nadler [c,1]

[a] Faculty of Mechanical Engineering, Technion-Israel Institute of Technology, 32000 Haifa, Israel
[b] Department of Structural and Geotechnical Engineering, Sapienza University of Rome, Rome, 00184, Italy
[c] Department of Mechanical Engineering, University of Victoria, Victoria, British Columbia, Canada

ARTICLE INFO

Keywords:
Continuum model
Granular materials
Jamming
$\mu(I)$ rheology
Smooth elastic–inelastic transition

ABSTRACT

A continuum model for granular materials, which transitions from an elastic jammed phase to rapid flows, is developed using a large deformation Eulerian formulation for compressible elastic-viscoplastic response. The model incorporates constitutive functions capturing $\mu(I)$ rheology, the value of the solid fraction developed for steady-state shearing, and the transient response for shear reversal based on experiments and simulations of interacting particles using the Discrete Element Method (DEM). The present model exhibits hyperelastic response with the stress determined by measures of elastic dilatation and elastic distortional deformations. This causes the stress to naturally have a direction different from the rate of deformation tensor for transient response. Examples examine pure dilation, steady-state simple shear, transient shearing with shear reversal for constant volume and constant non-shearing components of stress, and the transient transition to jamming.

1. Introduction

Granular materials are ubiquitous in nature and engineering applications, such as soils, powders, pharmaceuticals, and food products. They are systems formed by discrete particles, which can have different shapes and sizes, that interact through normal and shear contact forces [1]. This special microstructure conveys a response that transitions from solid-like elastic response with high solid fractions, to fluid-like flowing behavior for moderate rates and solid fractions, to gas-like behavior for high rates and low solid fractions [2].

The introduction of an external load to granular materials results in an uneven distribution of filamentary force chains depending on the unique shapes and arrangement of particles [3,4]. Techniques such as photoelastic force measurements, extensively applied for both qualitative and quantitative assessments of these forces, underscore their sensitivity to the regularity of particle shapes [5–8]. A macroscopic manifestation of these force chains is observed in the transition from a fluid-like state to a solid-like elastic state, a phenomenon known as *jamming* [9]. Jamming occurs when particles are densely packed or subjected to sufficient pressure, leading to a configuration where they are nearly immobilized and form an elastic structure. Additionally, shear stress application can induce jamming by prompting particles to rearrange, forming force chains that impede further flow [10].

To characterize the transition from a jammed solid-like state to a fluid-like state, especially under conditions of high solid fractions and low rates of deformation, many works have made use of additional internal-state variables called a *fabric tensor*, or a coordination number, that represent local inter-grain contacts which give rise to inter-grain contact forces. In this spirit, [11] extensively explored various definitions of the fabric tensor and their effects on the solid-like to fluid-like transition. A history-dependent viscosity tensor was used in [12], and a rate-independent hypoplastic model has been generalized to include dilatancy with a fabric tensor based on an evolution equation in [13]. A thermomechanical approach was used in [14] to construct elastic–plastic models for soils and sands. This approach provided a rigorous derivation of the yield condition, flow rule, and dissipation function, making important distinctions between the rates of plastic work and plastic dissipation, often assumed to be equal in existing soil mechanics theories. Employing a hyperplasticity theory, [15] proposed a formulation that incorporates isotropic and rotational hardening, providing insights into two distinct manifestations of isotropic and anisotropic elastic–plastic coupling, with a specific focus on clays. Interestingly, [16] presented a phase diagram for jammed materials, offering a statistical description of jammed states wherein random close packing is interpreted as the ground state of the ensemble of jammed matter. In this paper, the term jamming signifies the point at which the

* Corresponding author.
E-mail addresses: mbrubin@tx.technion.ac.il (M.B. Rubin), jacopo.ciambella@uniroma1.it (J. Ciambella), bnadler@uvic.ca (B. Nadler).
[1] All authors contributed equally to all aspects of this joint paper.

https://doi.org/10.1016/j.ijmecsci.2024.109391
Received 29 September 2023; Received in revised form 25 April 2024; Accepted 13 May 2024
Available online 18 May 2024

material ceases to flow inelastically and the response is characterized by that of an elastic solid. Recent experiments by [17] specifically addressed the fluidization response of granular media in proximity to the jamming solid–fluid transition. Notably, several studies, such as [18,19], adopt a parallel approach to model stresses in granular materials. This approach involves considering both stresses generated by force chains and an additional contribution due to interparticle collisions. The latter contribution is typically modeled using the concept of granular temperature, which reflects the kinetic energy of the particles. However, this kinetic theory-based approach is not employed in the present study.

Some continuum models utilized non-Newtonian fluid mechanics to model compressible granular materials [20,21], specifically addressing the fluid-flow region. Additionally, [22] extended the scope by generalizing depth-integrated viscous terms in continuum equations, developing $\mu(I)$ rheology for dense granular flows. A study by [23] proposed, and numerically implemented, a constitutive framework for granular media that allows the material to traverse through its many common phases during the flow process. When dense, the material is treated as a pressure-sensitive elasto-viscoplastic solid obeying a yield criterion and a plastic flow rule given by the $\mu(I)$ inertial rheology of granular materials. When the solid volume fraction drops below a critical level, the material is allowed to pull apart and is treated as a stress-free media. In [24] an elastic–plastic model using a Lagrangian formulation was developed that captures $\mu(I)$ rheology and numerous numerical simulations for steady-state flows were analyzed.

The advent of powerful computers with large memories has enabled the use of microscopic discrete simulations, notably the Discrete Element Method (DEM), to dynamically calculate systems of interacting particles with arbitrary shapes [25]. In DEM simulations, the dynamical equations for each particle are solved, assuming functional forms for the contact forces (normal and shear) that characterize particle interactions. These contact forces are often modeled as soft contacts, allowing particles to interpenetrate. The analysis of data from DEM simulations has unveiled scaling laws for various quantities and functional forms for the steady-state value ϕ_c of the solid fraction, as evidenced by [26] and [27]. DEM simulations have also been instrumental in studying the jamming transition, as demonstrated by [28]. However, it is crucial to note that constitutive modeling of contact forces in DEM simulations is an active research area, as highlighted by [29]. While DEM simulations provide valuable insights into the underlying physics of granular materials, their feasibility diminishes for large-scale systems, where continuum approaches become essential.

The objective of this paper is to develop a continuum model of granular materials for the full range of response from a jammed elastic solid to a flowing material. Specifically, an Eulerian formulation of constitutive equations for compressible elastic-viscoplastic response, which exhibit a continuity of solid and fluid states [30] and exhibit a smooth elastic–inelastic transition [31,32], is enriched with known functional forms for granular materials. Evolution equations for internal state history-dependent variables in the model are inspired by empirical functional forms, that capture important observations in DEM simulations of interacting particles. The present model exhibits hyperelastic response with the stress determined by measures of elastic dilatation and elastic distortional deformations. This causes the stress to naturally have a direction different from the rate of deformation tensor for transient response. In particular, the proposed model includes functional forms for $\mu(I)$ rheology in [21,22], for the steady-state solid fraction ϕ_c in [27] and modifications for the response near jamming discussed in [26]. Furthermore, although the proposed model includes solid-like response, it is fully Eulerian in the sense that there is no dependence on arbitrary specifications of total and plastic deformation measures and reference and intermediate configurations. Consequently, the steady-state response depends only on the current state of the material and not on the history of the response that led to steady-state. This approach is different from more standard approaches that determine the stress based on the rate of deformation tensor, coordination numbers, and history-dependent fabric tensors as in [33–35].

Table 1
List of Latin symbols, equations and descriptions.

Parameter	Eqn.	Description
a_i	(28)	Constants in the evolution equation for ϕ_s
a_c	(26)	Constant in the function ϕ_c
$\mathbf{A}_p$	(9)	Direction of the inelastic deformation rate
b_c	(26)	Constant in the function ϕ_c
b_{ij}	(45)	Components of $\bar{\mathbf{B}}_e$
$\bar{\mathbf{B}}_e$	(9)	Elastic distortional deformation
C	(32)	Constant in the function Γ
d	(23)	Length parameter related to the particle diameter
$\mathbf{D}$	(1)	Rate of deformation
D'_{ij}	(70)	Components of $\mathbf{D}'$
$\mathbf{D}'^*$	(39)	Modified rate of distortional deformation
$\mathcal{D}$	(11)	Total rate of material dissipation
$\mathcal{D}_d$	(14)	Dissipation due to inelastic distortional deformation
$\mathcal{D}_\phi$	(14)	Dissipation due to changes in the solid fraction
$\mathbf{e}_i$	(43)	Fixed orthonormal base vectors
g	(32)	Yield function
$\mathbf{g}'_e$	(33)	Elastic distortional strain
G_s	(18)	Shear modulus of the granular material
H	(84)	Thickness of the shearing layer
I	(23)	Inertial number
I^*	(40)	Modified inertial number
$\mathbf{I}$	(2)	Second order identity tensor
I_0	(24)	Constant defining the function $\mu(I)$

Table 2
List of Latin symbols, equations and descriptions (continued).

Parameter	Eqn.	Description
J	(60)	Total dilatation
J_{se}	(4)	Elastic dilatation of the solid particles
k	(67)	Stiffness of the contact springs
k_s	(19)	Determines the bulk modulus of the granular material
L	(43)	Value of the shearing rate
$\mathbf{L}$	(1)	Velocity gradient
m	(48)	Auxiliary parameter
p	(13)	Pressure
p^*	(38)	Normalized value of p
$\mathbf{T}$	(11)	Cauchy stress
T_{12}	(63)	Shear component of $\mathbf{T}$
u	(82)	Shear displacement
$\mathbf{v}$	(1)	Velocity of a material point
$\mathbf{x}$	(1)	Position of a material point

An outline of the paper is as follows. Sections 2 and 3 present the general and specific constitutive equations for the model, respectively. Section 4 presents a summary of the model equations and Section 5 discusses examples of pure dilation, steady-state shear, transient shearing with shear reversal for constant volume and constant non-shearing components of stress, and the transient smooth transition to jamming. Section 6 presents conclusions. Since there are a number of variables used to capture the complicated response of granular materials, Tables 1, 2, 3 summarize all variables, the equations where they are introduced or defined and a brief description of their meanings.

2. General constitutive equations

The objective of this section is to summarize the Eulerian formulation of the model for elastically isotropic elastic–inelastic response used to model granular material. This model introduces a strain energy function that depends on an elastic dilatation and an elastic distortional deformation tensor. Motivated by the work in [36,37], these elastic deformation measures are determined directly by evolution equations that include rates of inelasticity. The stress is determined by hyperelastic constitutive equations in terms of these elastic deformation measures. These equations are Eulerian in the sense that they are insensitive to arbitrary specifications of reference and intermediate configurations

Table 3
List of Greek symbols, operators, equations and descriptions.

Parameter	Eqn.	Description
α_1	(10)	First invariant of elastic distortional deformation
α_2	(10)	Second invariant of elastic distortional deformation
$\dot{\beta}$	(38)	Shearing rate
$\dot{\beta}^*$	(38)	Normalized shearing rate $\dot{\beta}$
γ	(46)	Auxiliar parameter
γ_e	(33)	Measure of elastic distortional strain
γ_m	(49)	Steady-state value of γ
Γ	(32)	Controls the inelastic deformation rate
Γ_J	(62)	Controls the rate of evolution of ϕ_J
$\dot{\varepsilon}$	(31)	Equivalent total distortional deformation rate
ε_v	(7)	Elastic volume compression
ζ_1	(25)	Angle defining μ_1
ζ_2	(25)	Angle defining μ_2
κ	(32)	hardening variable
κ_c	(51)	Value of κ determining the elastic limit
κ_m	(51)	Steady-state value of κ
$\mu(I)$	(24)	Coefficient for $\mu(I)$ rheology
$\mu(I^*)$	(42)	Modified value of $\mu(I)$ rheology
μ_1	(25)	Constant defining the function $\mu(I)$
μ_2	(25)	Constant defining the function $\mu(I)$
ν_s	(19)	Poisson's ratio of the solid particles
ρ	(3)	Mass density of the granular material
ρ_b	(82)	Mass density per unit area
ρ_s	(3)	Current density of the particles
ρ_{sz}	(4)	zero-stress density of the particles
ϕ_c	(26)	Function for the steady-state value of ϕ_s
ϕ_J	(28)	jamming value of ϕ_s
ϕ_s	(3)	Solid volume fraction
Σ	(11)	Strain energy per unit mass
$\dot{(\,)}$	(1)	Material derivative
$(\,)'$	(2)	Deviatoric part of a tensor
$\mathbf{A}\cdot\mathbf{B}$	(2)	Inner product of two tensors
$\mathbf{a}\otimes\mathbf{b}$	(43)	Tensor product between two vectors
$\langle x\rangle$	(8)	Macaulay brackets

as well as total and plastic strain measures [38]. Even though elastic strains remain small for granular materials, the constitutive equations must be properly invariant under superposed rigid body motions to be able to model the large total deformations of a flowing material.

2.1. Kinematics

A material point located in the present configuration by the vector $\mathbf{x}$ has velocity $\mathbf{v}$, gradient of velocity $\mathbf{L}$ and rate of deformation $\mathbf{D}$ defined by

$$\mathbf{v}=\dot{\mathbf{x}},\quad \mathbf{L}=\partial\mathbf{v}/\partial\mathbf{x},\quad \mathbf{D}=\frac{1}{2}(\mathbf{L}+\mathbf{L}^T), \tag{1}$$

where $\dot{(\,)}$ denotes material time differentiation. Also, the deviatoric part of a tensor is denoted by $(\,)'$, so for example

$$\mathbf{L}'=\mathbf{L}-\frac{1}{3}(\mathbf{L}\cdot\mathbf{I})\mathbf{I}, \tag{2}$$

where $\mathbf{I}$ is the second order identity tensor and $\mathbf{A}\cdot\mathbf{B}=\mathrm{tr}(\mathbf{A}\mathbf{B}^T)$ is the inner product of two second order tensors $\mathbf{A},\mathbf{B}$.

2.2. Evolution equation for the elastic dilatation

Following the work in [39] a granular material has mass density ρ and solid volume fraction ϕ_s in the current configuration. Moreover, ρ_s is the density of the solid particles in the current configuration. Assuming that the pore space is evacuated, it follows that the current density ρ of the granular media is given by

$$\rho=\phi_s\rho_s, \tag{3}$$

and the elastic dilatation J_{se} of the solid particles is defined by

$$J_{se}=\frac{\rho_{sz}}{\rho_s},\quad \rho=\rho_{sz}J_{se}^{-1}\phi_s, \tag{4}$$

where ρ_{sz} is the zero-stress density of the solid particles. Next, using the conservation of mass of the granular material

$$\dot{\rho}+\rho(\mathbf{D}\cdot\mathbf{I})=0, \tag{5}$$

it follows that the elastic dilatation J_{se} satisfies the evolution equation

$$\frac{\dot{J}_{se}}{J_{se}}=\mathbf{D}\cdot\mathbf{I}+\frac{\dot{\phi}_s}{\phi_s}, \tag{6}$$

which indicates that the rate of elastic dilation of the solid particles, $\dot{J}_{se}$, is determined by the influences of the total dilatation rate and the rate of solid volume fraction change, $\dot{\phi}_s$. Eq. (6) requires the specification of an evolution equation for $\dot{\phi}_s$. This elastic dilatation is greater than unity for expanded states $J_{se}>1$ and is less than unity for compressed states $J_{se}<1$. For states where $J_{se}>1$, the particles are not compressed due to contacts, and the pressure vanishes. Hence, it is convenient to introduce the volumetric compressive strain ε_v by the expression

$$\varepsilon_v=\langle 1-J_{se}\rangle, \tag{7}$$

where the Macaulay brackets are defined by

$$\langle x\rangle=\max(x,0). \tag{8}$$

These Macaulay brackets have been used to cause the pressure (positive in compression) to vanish when the granular material is expanded sufficiently for the particles to lose contact with each other.

2.3. Evolution equation for the elastic distortional deformation

Motivated by the work in [40] the elastic distortional deformation $\bar{\mathbf{B}}_e$ of the granular material is a symmetric, unimodular, positive-definite tensor which satisfies the evolution equation

$$\dot{\bar{\mathbf{B}}}_e=\mathbf{L}'\bar{\mathbf{B}}_e+\bar{\mathbf{B}}_e\mathbf{L}'^T-\Gamma\mathbf{A}_p,\quad \mathbf{A}_p=\bar{\mathbf{B}}_e-\Big(\frac{3}{\bar{\mathbf{B}}_e'^{-1}\cdot\mathbf{I}}\Big)\mathbf{I}, \tag{9}$$

where $\Gamma\geq 0$ is a function that controls the magnitude of the inelastic deformation rate and needs to be specified by a constitutive equation. Also $\mathbf{A}_p$ controls the direction of the inelastic deformation rate and satisfies the condition $\mathbf{A}_p\cdot\bar{\mathbf{B}}_e^{-1}=0$, which ensures that $\bar{\mathbf{B}}_e$ remains unimodular. Moreover, the first invariant α_1 of the elastic distortion $\bar{\mathbf{B}}_e$ satisfies the equations

$$\alpha_1=\bar{\mathbf{B}}_e\cdot\mathbf{I},\quad \dot{\alpha}_1=2\bar{\mathbf{B}}_e'\cdot\mathbf{D}-\Gamma\mathbf{A}_p\cdot\mathbf{I}. \tag{10}$$

For general elastically isotropic response the strain energy should include the second invariant $\alpha_2=\bar{\mathbf{B}}_e\cdot\bar{\mathbf{B}}_e$ of $\bar{\mathbf{B}}_e$, but this is not used for simplicity. Also, for an elastic process with $\Gamma=0$ from an initially zero-stress state with $\bar{\mathbf{B}}_e=\mathbf{I}$, the evolution Eq. (9) integrates to obtain $\bar{\mathbf{B}}_e$ equal to the unimodular part of the left Cauchy–Green deformation tensor.

2.4. General constitutive equation for stress

For the purely mechanical theory, the rate of material dissipation D requires

$$D=\mathbf{T}\cdot\mathbf{D}-\rho\dot{\Sigma}\geq 0, \tag{11}$$

where the specific (per unit mass) strain energy function of the granular material Σ is taken in the form

$$\Sigma=\Sigma(\varepsilon_v,\alpha_1), \tag{12}$$

and the stress is specified by

$$\mathbf{T}=-p\mathbf{I}+\mathbf{T}',\quad p=\phi_s\rho_{sz}\frac{\partial\Sigma}{\partial\varepsilon_v},\quad \mathbf{T}'=\frac{2\phi_s}{1-\varepsilon_v}\rho_{sz}\frac{\partial\Sigma}{\partial\alpha_1}\bar{\mathbf{B}}_e', \tag{13}$$

where $\mathbf{T}'$ is the deviatoric stress, p is the pressure and use has been made of (3)–(4), (6) and (10). This specification of stress is made to ensure that when $\Gamma=0$ the model reproduces hyperelastic response. Also, the Cauchy stress for uniaxial stress is positive in tension.

2.5. Rates of material dissipation

Using the definitions (4), (7), the constitutive Eqs. (13) and the evolution Eqs. (6) and (10), the rate of material dissipation (11) can be written in the form

$$\mathcal{D} = \mathcal{D}_d + \mathcal{D}_\phi, \quad \mathcal{D}_d = \frac{\phi_s}{1-\varepsilon_v}\Gamma\rho_{sz}\frac{\partial\Sigma}{\partial\alpha_1}(\mathbf{A}_p\cdot\mathbf{I}), \quad \mathcal{D}_\phi = p\,\frac{\dot\phi_s}{\phi_s}, \tag{14}$$

where $\mathcal{D}_d$ is the dissipation rate due to inelastic distortional deformation and $\mathcal{D}_\phi$ is the dissipation rate due to changes in solid fraction. Furthermore, the strain energy is specified to satisfy the restrictions

$$\begin{aligned} &\Sigma = 0, \qquad \frac{\partial\Sigma}{\partial\varepsilon_v} = 0, \quad \text{for} \quad \varepsilon_v = 0, \bar{\mathbf{B}}_e = \mathbf{I}, \\ &\frac{\partial^2\Sigma}{\partial\varepsilon_v^2} > 0, \quad \frac{\partial\Sigma}{\partial\alpha_1} > 0, \end{aligned} \tag{15}$$

which cause the strain energy to vanish for a zero-stress state with $\varepsilon_v = 0, \bar{\mathbf{B}}_e = \mathbf{I}$ and cause the effective bulk and shear moduli to be positive.

By expressing $\bar{\mathbf{B}}_e$ in its spectral form it was shown in [40] that

$$\mathbf{A}_p\cdot\mathbf{I} = \bar{\mathbf{B}}_e\cdot\mathbf{I} - \frac{9}{\bar{\mathbf{B}}_e^{-1}\cdot\mathbf{I}} \geq 0, \tag{16}$$

which together with the restriction (15) on the shear modulus ensures that the rate of inelastic distortional deformation is dissipative

$$\mathcal{D}_d \geq 0. \tag{17}$$

The total rate of material dissipation (14) must be non-negative $\mathcal{D} \geq 0$. In the next section an evolution equation for $\dot\phi_s$ is specified which allows $\mathcal{D}_\phi$ to be positive or negative while ensuring that $\mathcal{D} \geq 0$.

3. Specific constitutive equations

The objective of this section is to propose specific constitutive equations with functions that are calibrated to models of $\mu(I)$ rheology for steady-state flows and observations from DEM simulations.

3.1. A specific form for the strain energy function

The strain energy function is specified by the compressible Neo-Hookean form

$$\rho_{sz}\Sigma = G_s\big[-k_s\{\varepsilon_v + \ln(1-\varepsilon_v)\} + \frac{1}{2}(\alpha_1 - 3)\big]. \tag{18}$$

The term in Σ depending on the elastic compression ε_v controls the response to compression, with $k_sG_s > 0$ being the zero-stress bulk modulus, and the term in Σ depending on α_1 controls the response to the elastic distortional deformation, with $G_s > 0$ being the zero-stress shear modulus of the granular material. Also, assuming the solid particles are elastically isotropic, the normalized bulk modulus k_s is determined by the zero-stress Poisson's ratio ν_s of the solid particles by

$$k_s = \frac{2(1+\nu_s)}{3(1-2\nu_s)}, \tag{19}$$

Then, with the help of (13) the stresses associated with (18) are given by

$$p = \frac{\phi_s}{1-\varepsilon_v}G_sk_s\varepsilon_v \geq 0, \quad \mathbf{T}' = \frac{\phi_s}{1-\varepsilon_v}G_s\bar{\mathbf{B}}_e'. \tag{20}$$

It is emphasized that the elastic measures ε_v and $\bar{\mathbf{B}}_e'$ are used here instead of the *coordination number* and *fabric tensor* in [35]. Further inspection of (20) suggest that ε_v is related to the *coordination number* controlling the pressure and $\bar{\mathbf{B}}_e'$ is related to the traceless *fabric tensor* controlling the deviatoric stress.

Furthermore, from (9) it can be shown that

$$\dot{\bar{\mathbf{B}}}_e' = \mathbf{L}'\bar{\mathbf{B}}_e + \bar{\mathbf{B}}_e\mathbf{L}'^T - 2(\bar{\mathbf{B}}_e\cdot\mathbf{D}')\mathbf{I} - \Gamma\bar{\mathbf{B}}_e', \tag{21}$$

and for small elastic distortional deformations $\bar{\mathbf{B}}_e \approx \mathbf{I}$ so this equation can be approximated by

$$\dot{\bar{\mathbf{B}}}_e' = 2\mathbf{D}' - \Gamma\bar{\mathbf{B}}_e'. \tag{22}$$

This indicates that the stress $\mathbf{T}'$ is proportional to the deviatoric rate of deformation $\mathbf{D}'$ for steady-state response ($\dot{\bar{\mathbf{B}}}_e' = 0$) but not for transient response ($\dot{\bar{\mathbf{B}}}_e' \neq 0$).

3.2. $\mu(I)$ Rheology

The proposed model is developed to simulate the deviatoric stress and the solid volume fraction predicted by the $\mu(I)$ rheology model for steady-state flow. From [21,22] it is recalled that for $\mu(I)$ rheology of granular materials, the deviatoric stress is expressed in the form

$$\mathbf{T}' = \sqrt{2}\,\mu(I)p\frac{\mathbf{D}'}{|\mathbf{D}'|}, \quad I = \frac{\sqrt{2}\,|\mathbf{D}'|d}{\sqrt{\frac{p}{\rho}}} = \frac{\sqrt{2}\,|\mathbf{D}'|d}{\sqrt{\frac{G_sk_s\varepsilon_v}{\rho_{sz}}}}, \tag{23}$$

where $|\mathbf{D}'| = \sqrt{\mathbf{D}'\cdot\mathbf{D}'}$, I is the inertial number, d has the dimensions of length, which represents the particle size, and the phenomenological function $\mu(I)$ is defined by

$$\mu(I) = \mu_1 + \frac{\mu_2 - \mu_1}{1 + \frac{I_0}{I}}. \tag{24}$$

In this expression I_0 is a constant and μ_1 and μ_2 are defined by

$$\mu_1 = \tan\zeta_1, \quad \mu_2 = \tan\zeta_2, \tag{25}$$

where ζ_1 and ζ_2 are the constant minimum and maximum friction slope angles.

There seems to be some confusion in the literature about whether p in (23) is the pressure in the granular media, as defined in [[21], Eq. (3)] and in [[22], Eqs. (2.8), (2.9)], or is the normal compression applied to a shearing layer as in [[21], Fig. 1]. To be definite, in this paper p is the pressure in the granular media.

The function ϕ_c is motivated by the model in [27]

$$\phi_c = \frac{\phi_J}{1 + \frac{a_c}{\phi_J}I^{b_c}} > 0, \tag{26}$$

where the inertial number I is defined in (24), and a_c and b_c are non-negative constants, and ϕ_J $(1 > \phi_J > 0)$ is a constant that represents the critical solid volume fraction at the onset of jamming. It should be noted that ϕ_c is equal to the jamming value ϕ_J when $I = 0$. For steady-state with small values of I this form is the same as that in [27]. Specifically, this functional form has been modified relative to that in [27] to ensure that ϕ_c approaches zero for large values of I, while remaining non-negative. Also, these evolution equations ensure that ϕ_s remains in the range

$$0 < \phi_s \leq \phi_J < 1. \tag{27}$$

3.3. Evolution equation for the solid volume fraction

This model limits attention to states of a granular material with positive pressure (i.e. $p > 0$) which maintains particle contacts. The rate of material dissipation $\mathcal{D}_\phi$ in (14) due to solid fraction changes will be non-negative for porous compaction *i.e.* $\dot\phi_s > 0$ at positive pressure $p > 0$. However, *bulking* is identified with porous dilation *i.e.* $\dot\phi_s < 0$ at positive pressure p, which tends to cause negative dissipation. Consequently, the evolution equation for solid fraction during bulking must be restricted so that the total rate of material dissipation D remains non-negative.

To satisfy these restrictions, and motivated by the work in [41] the evolution equation for ϕ_s is proposed in the form

$$\begin{aligned}\frac{\dot{\phi}_s}{\phi_s} &= \exp\Big[-a_1\Big(\frac{\phi_s}{\phi_J-\phi_s}\Big)\Big]\langle -\mathbf{D}\cdot\mathbf{I}\rangle \\ &\quad -\Big[\frac{\big(\frac{a_2}{\sqrt{\varepsilon_v}}\big)\langle\phi_s-\phi_c\rangle}{G_s k_s+\big(\frac{a_2}{\sqrt{\varepsilon_v}}\big)\langle\phi_s-\phi_c\rangle\, p}\Big]\mathcal{D}_d \\ &\quad +\Gamma(a_3+a_4\langle -\mathbf{D}\cdot\mathbf{I}\rangle)\varepsilon_v\langle\phi_c-\phi_s\rangle,\end{aligned} \tag{28}$$

where the maximum value of ϕ_s is limited to ϕ_J which is the onset of jamming. More specifically, ϕ_s is a measure of the particle packing. The term associated with volumetric compression $\langle -\mathbf{D}\cdot\mathbf{I}\rangle$ tends to cause the solid fraction ϕ_s to increase (compaction of the particle packing) towards the jamming value ϕ_J with the rate of the transition controlled by the constant $a_1 \geq 0$. The example of dilatation in Section 5.1 examines the influence of a_1. The rate of distortional dissipation $\mathcal{D}_d$ tends to cause the solid fraction ϕ_s to evolve towards the function ϕ_c, which characterizes the steady-state value of ϕ_s, with the rate of the transition controlled by the constant $a_2 \geq 0$. This term, which is active only during inelastic distortional deformation, causes ϕ_s to decrease when $\phi_s > \phi_c$ and to increase when $\phi_s < \phi_c$, as can be seen in Figs. 3b and 5b. This increase in ϕ_s at positive pressure is denoted as *bulking*, which is similar to what can occur in porous rock [42]. The last term on the right-hand-side of (28) tends to cause ϕ_s to increase towards ϕ_c when $\phi_c > \phi_s$ with the transition controlled by the constants $a_3 \geq 0, a_4 \geq 0$. This increase in ϕ_s stops when $\varepsilon_v = 0$ and the pressure vanishes. Also, that dependence of this term on $\langle\mathbf{D}\cdot\mathbf{I}\rangle$ and the constant a_4 are necessary to obtain the good correspondence with the result of the DEM simulation discussed in Section 5.4.2.

From (14) it can be seen that increase in ϕ_s is dissipative $\mathcal{D}_\phi > 0$ and that decrease in ϕ_s is not dissipative $\mathcal{D}_\phi < 0$. Consequently, the coefficient of the term associated with $\mathcal{D}_d$ is specified to ensure that the total dissipation remains non-negative $\mathcal{D} \geq 0$. Specifically, using these expressions, the total dissipation rate due to inelastic distortional deformation rate and due to solid fraction changes in (14) is given by

$$\begin{aligned}\mathcal{D} &= p\,\exp\Big[-a_1\Big(\frac{\phi_s}{\phi_J-\phi_s}\Big)\Big]\langle -\mathbf{D}\cdot\mathbf{I}\rangle \\ &\quad +\Big[\frac{G_s k_s}{G_s k_s+\big(\frac{a_2}{\sqrt{\varepsilon_v}}\big)\langle\phi_s-\phi_c\rangle\, p}\Big]\mathcal{D}_d \\ &\quad +\Gamma(a_3+a_4\langle -\mathbf{D}\cdot\mathbf{I}\rangle)\varepsilon_v\langle\phi_c-\phi_s\rangle\, p \geq 0.\end{aligned} \tag{29}$$

This form ensures that the rate of material dissipation due to inelastic distortional deformation rate dominates the non-dissipation due to bulking so that the restriction (29) is automatically satisfied. Furthermore, with the help of (14), (16) and (18) the expression for $\mathcal{D}_d$ is given by

$$\mathcal{D}_d = \frac{\phi_s}{1-\varepsilon_v}\Gamma G_s \mathbf{A}_p\cdot\mathbf{I} \geq 0. \tag{30}$$

3.4. A constitutive equation for Γ

Following the work in [31] for a model with a smooth elastic–inelastic transition, the equivalent total distortional deformation rate $\dot{\varepsilon}$ is defined by

$$\dot{\varepsilon} = \sqrt{\frac{2}{3}\mathbf{D}'\cdot\mathbf{D}'}, \tag{31}$$

and a modified form of the function Γ, which controls the rate of inelastic deformation in (32), is specified by

$$\Gamma = \frac{3}{2C\kappa}\dot{\varepsilon}\langle g\rangle, \quad g = 1-\frac{(1-C)\kappa}{\gamma_e}, \quad 0<C<1, \tag{32}$$

where g is a yield function, the equivalent elastic distortional strain γ_e is defined by

$$\gamma_e = \sqrt{\frac{3}{2}\,\mathbf{g}'_e\cdot\mathbf{g}'_e}, \quad \mathbf{g}'_e = \frac{1}{2}\bar{\mathbf{B}}'_e, \tag{33}$$

κ is an equivalent elastic distortional yield strain, and the constant C controls the amount of overstress. Also, with the help of (20), (23) and (33) it can be shown that for $\mu(I)$ rheology

$$2\Big(\frac{\phi_s G_s}{1-\varepsilon_v}\Big)\gamma_e = \sqrt{3}\mu(I)p. \tag{34}$$

The expression (32) for Γ was motivated by the small elastic deformation steady-state response. Specifically, for small elastic deformations the evolution Eq. (9) for $\bar{\mathbf{B}}_e$ can be approximated by

$$\dot{\mathbf{g}}'_e = \mathbf{D}' - \Gamma\mathbf{g}'_e. \tag{35}$$

Next, with the help of (31)–(33) the steady-state solution of (35) during loading yields the results

$$\mathbf{D}' = \Gamma\mathbf{g}'_e, \quad \dot{\varepsilon} = \frac{2}{3}\Gamma\gamma_e = \frac{\dot{\varepsilon}\gamma_e}{C\kappa}\Big[1-\frac{(1-C)\kappa}{\gamma_e}\Big], \tag{36}$$

which requires

$$\gamma_e = \kappa \quad \text{for steady-state.} \tag{37}$$

Thus, the constitutive Eq. (32) causes the onset of yield to occur when $\gamma_e = (1-C)\kappa$ with a smooth transition to steady response $\gamma_e = \kappa$ for monotonic loading.

3.5. A modification for the response near jamming

[26] studied the response near jamming and showed that in the limit $\phi_s \to \phi_J$ the data for $\phi_J \geq \phi_s$ collapses to a single curve when p and the shearing rate $\dot{\beta}$ are replaced by p^* and $\dot{\beta}^*$, which are defined by

$$p^* = \frac{p}{(\phi_J-\phi_s)^{2/3}}, \quad \dot{\beta}^* = \frac{\dot{\beta}}{(\phi_J-\phi_s)^{4/3}}, \tag{38}$$

where it is noted that the expressions in [26] are written in terms of the void fraction $1-\phi_s$. This suggests that $\mathbf{D}'^*$ be defined by

$$\mathbf{D}'^* = \frac{\mathbf{D}'}{|\phi_J-\phi_s|^{4/3}}. \tag{39}$$

Next, with the help of I in (24) the modified value I^* of I is defined by

$$I^* = \frac{\phi_J}{\phi_J-\phi_s}I. \tag{40}$$

The numerator is specified so that I^* approaches I for small solid fractions $\phi_s \to 0$. Now, with the help of p^* in (38) and $\mathbf{D}'^*$ in (39) this form of I^* can be rewritten as

$$I^* = \frac{\phi_J}{\phi_J-\phi_s}\frac{\sqrt{2}(\phi_J-\phi_s)^{4/3}|\mathbf{D}'^*|d}{\sqrt{\frac{(\phi_J-\phi_s)p^*}{\rho}}} = \phi_J\frac{\sqrt{2}|\mathbf{D}'^*|d}{\sqrt{\frac{p^*}{\rho}}}. \tag{41}$$

This shows that I^* is consistent with the observations in [26] near the jamming limit. Moreover, this suggests that $\mathbf{T}'$ in (23) is replaced by

$$\mathbf{T}' = \sqrt{2}\mu(I^*)p\frac{\mathbf{D}'}{|\mathbf{D}'|}, \quad \mu(I^*) = \mu_1 + \frac{\mu_2-\mu_1}{1+\frac{I_0}{I^*}}. \tag{42}$$

These modifications improve the performance of the model for the transitions between solid and fluid responses near jamming, where the $\mu(I)$ rheology does not perform well.

3.6. A constitutive equation for κ

To develop a constitutive equation for κ, use is made of an exact solution for steady-state simple shear for which

$$\mathbf{L} = L\,\mathbf{e}_1\otimes\mathbf{e}_2, \quad \dot{\varepsilon} = \frac{L}{\sqrt{3}}, \tag{43}$$

where $L > 0$ controls the shearing rate, $\mathbf{e}_i$ is a fixed orthonormal triad of vectors and $\mathbf{a}\otimes\mathbf{b}$ denotes the tensor product of the two vectors $\mathbf{a}$ and

b. For simple shear the deformation is isochoric $\mathbf{D}\cdot\mathbf{I}=0$ and it follows from (6) that

$$\frac{d}{dt}\Big[\frac{\phi_s}{1-\varepsilon_v}\Big]=0, \tag{44}$$

even when the solid fraction ϕ_s is not constant due to elastic dilatation of the particles. Also, the pressure p and deviatoric stress $\mathbf{T}'$ are given by (20).

Next, from [43] the steady-state solution of (9) for simple shear is given by

$$\begin{aligned}
&\bar{\mathbf{B}}_e = b_{11}\mathbf{e}_1\otimes\mathbf{e}_1 + b_{22}(\mathbf{e}_2\otimes\mathbf{e}_2+\mathbf{e}_3\otimes\mathbf{e}_3) + b_{12}(\mathbf{e}_1\otimes\mathbf{e}_2+\mathbf{e}_2\otimes\mathbf{e}_1),\\
&\bar{\mathbf{B}}'_e = b'_{22}(-\frac{1}{2}\mathbf{e}_1\otimes\mathbf{e}_1+\mathbf{e}_2\otimes\mathbf{e}_2+\mathbf{e}_3\otimes\mathbf{e}_3) + b_{12}(\mathbf{e}_1\otimes\mathbf{e}_2+\mathbf{e}_2\otimes\mathbf{e}_1),\\
&b_{11}=\frac{1+2\gamma^2}{(1+\gamma^2)^{1/3}},\quad b_{22}=\frac{1}{(1+\gamma^2)^{1/3}},\quad b_{12}=\frac{\gamma}{(1+\gamma^2)^{1/3}},\\
&b'_{22}=\frac{b_{22}-b_{11}}{3}=-\frac{2\gamma^2}{(1+\gamma^2)^{1/3}},\quad \gamma_e=\frac{\gamma\sqrt{3+4\gamma^2}}{2(1+\gamma^2)^{1/3}}.
\end{aligned} \tag{45}$$

where auxiliary parameter γ

$$L=\gamma\,\Gamma. \tag{46}$$

has been introduced to simplify the expressions (45).

Now, with the help of (20) and (42), for steady-state simple shear, the stress T_{12} is given by

$$T_{12}=\Big(\frac{\phi_s G_s}{1-\varepsilon_v}\Big)\frac{\gamma}{(1+\gamma^2)^{1/3}}=\mu(I^*)p=\mu(I^*)\phi_s G_s k_s\,\frac{\varepsilon_v}{1-\varepsilon_v}, \tag{47}$$

which can be rewritten in the form

$$\gamma^3-m\gamma^2-m=0,\quad m=\big[\mu(I^*)k_s\varepsilon_v\big]^3. \tag{48}$$

and solved to obtain

$$\begin{aligned}
\gamma=\gamma_m=\frac{m}{3}&+\frac{(108\ m+8m^3+12\ m\sqrt{81+12m^2}\,)^{1/3}}{6}\\
&+\frac{2m^2}{3(108\ m+8m^3+12\ m\sqrt{81+12m^2}\,)^{1/3}},
\end{aligned} \tag{49}$$

Next, using (32) and (43), Eq. (46) with $\gamma=\gamma_m$ requires

$$\frac{\sqrt{3}\gamma_m}{2C\kappa}\langle 1-\frac{(1-C)\kappa}{\gamma_e}\rangle=1, \tag{50}$$

which will yield the steady-state solution $\gamma_e=\kappa$ that is used to obtain the functional form of κ given by

$$\kappa=\max(\kappa_m,\kappa_c),\quad \kappa_m=\frac{\sqrt{3}\gamma_m}{2}, \tag{51}$$

where $(1-C)\kappa_c>0$ determines the finite elastic limit for low values of pressure. The constant κ_c determines the minimum value of κ which characterizes the *elastic limit for jamming*. To avoid confusion, I^* in (40) is used to determine γ_m in (49) and I in (23) is used to determine ϕ_c in (26).

4. Summary of the state variables, evolution equations, constitutive equations and material parameters

4.1. State variables and evolution equations

The history-dependent state variables in this model are the elastic dilatation J_{se}, the elastic distortional deformation tensor $\bar{\mathbf{B}}_e$ and the solid volume fraction ϕ_s, which are determined by the evolution Eqs. (6), (9) and (28), respectively, and need initial conditions

$$\big\{J_{se}(0),\bar{\mathbf{B}}_e(0),\phi_s(0)\big\}. \tag{52}$$

Table 4
List of parameters, equations, and references.

Parameter	Value	Eqn.	Reference
Strain energy function			
ρ_{sz} [kg/m^3]	2550	(4)	[22]
G_s [kPa]	10	(18)	None
ν_s	1/3	(19)	None
Inelastic transition parameter			
C	0.9	(32)	None
Parameters for $\mu(I)$ rheology			
d [mm]	0.1	(23)	[22]
I_0	0.01285	(24)	[35]
ζ_1 [Deg]	18.9	(25)	[22]
ζ_2 [Deg]	29.0	(25)	[22]
ϕ_J	0.64	(28)	[26]
Parameters for ϕ_c			
a_c	0.2161	(26)	None
b_c	0.20	(26)	None
Parameter for κ			
κ_c	1.0×10^{-5}	(51)	None
Parameters for the evolution of ϕ_s			
a_1	0.02	(28)	None
a_2	60.0	(28)	Optimized using [35]
a_3	40.0	(28)	Optimized using [35]
a_4 [s]	300	(28)	Optimized using [35]
Initial condition			
$\varepsilon_v(0)$	6.1147×10^{-3}	(7)	Optimized using [35]

4.2. Constitutive equations and material constants

The elastic response of the model is determined by the strain energy function Σ in (18) for compression of the solid grains and resistance of distortion of the granular media, which depends on the constant zero-stress density ρ_{sz}, and the zero-stress shear modulus G_s and normalized bulk modulus k_s

$$\big\{\rho_{sz},G_s,k_s\big\}, \tag{53}$$

The pressure p and the deviatoric Cauchy stress $\mathbf{T}'$ are given by (20). These stresses depend algebraically on the elastic compression ε_v, the elastic distortional deformation $\bar{\mathbf{B}}_e$ and the solid volume fraction ϕ_s. The function Γ in the evolution Eq. (9), which controls the rate of inelastic deformation, is specified by (32) with one constant

$$\big\{C\big\}, \tag{54}$$

with the effective elastic distortional deformation γ_e defined by (33) and the hardening function κ defined by (51). In the expression for γ_m in (49) the auxiliary function m is defined by (48). This function m is defined by five additional constants (the particle diameter d, the reference inertial number I_0, the friction angles ζ_1,ζ_2 and the jamming value ϕ_J of the solid fraction)

$$\big\{d,I_0,\zeta_1,\zeta_2,\phi_J\big\}, \tag{55}$$

where use is made of the expressions (25) for the friction coefficients μ_1,μ_2. Furthermore, the evolution Eq. (28) for the solid volume fraction ϕ_s has four additional constants

$$\big\{a_1,a_2,a_3,a_4\big\}, \tag{56}$$

the function ϕ_c in (26), which determines the steady-state value of ϕ_s, has two additional constants

$$\big\{a_c,b_c\big\}, \tag{57}$$

and the hardening parameter κ in (51) has another constant

$$\big\{\kappa_c\big\}, \tag{58}$$

that determines the *elastic limit of jamming*.

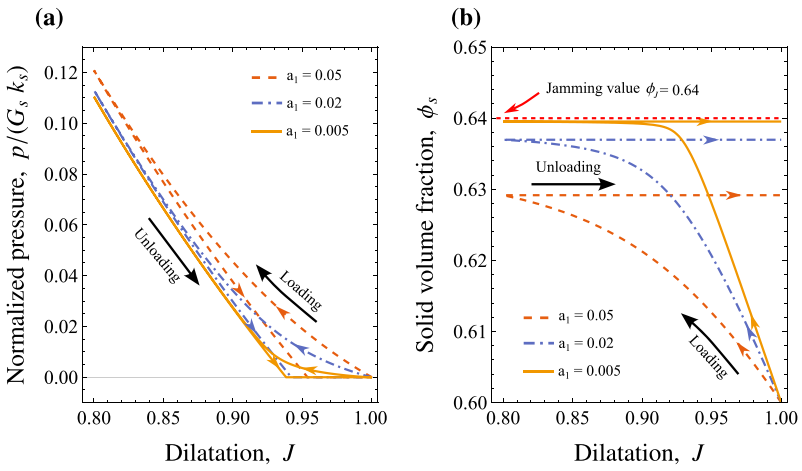

Fig. 1. Influence of the constitutive parameters: (a)–(b) Effects of varying a_1 on a pure dilatation response. The parameter a_1 controls the resistance of the granular material to compaction: for small values of a_1 the material compacts rapidly until the solid volume fraction ϕ_s approaches the jamming value $\phi_J = 0.64$.

Table 5
Initial values for steady-state simple shear.

Parameter	Value	Parameter	Value
$\dot{\gamma}_0$ [1/s]	0.758618	b_{12}	6.52235×10^{-3}
$b_{11} - 1$	7.09029×10^{-5}	$b_{22} - 1$	-1.41803×10^{-5}

5. Examples used to calibrate the material constants

A consistent set of material parameters for a single granular material was not found in the literature. Consequently, values are taken from different sources. Therefore, the set of material parameters used for the examples in this section shows the capabilities of the proposed model and not the response of a specific material. The complete set of reference parameters for dry spherical particles is listed in Table 4 along with the equation where the parameter is first introduced or defined as well as references when applicable.

For general deformations, the response of the material depends on nonlinear equations that couple the influences of the material constants. However, for the simple example of pure dilatation it is possible to isolate the influence of a_1. The values of a_2, a_3, a_4 in Table 4 were optimized by trial and error to match the simulations of transient shearing with shear reversal for constant volume and constant non-shearing components of stress reported in [[35], Figs. 1, 2]. Unless otherwise specified, the values of the parameters used in the examples are taken from Table 4 with initial values specified in Table 5. The value of G_s was specified arbitrarily and is used to normalize all stresses. Furthermore, it is noted that the Eulerian formulation yields steady-state solutions that depend only on the current state of the material. Specifically, they are independent of the initial conditions that lead to the steady-state.

5.1. Specification of a_1

Consider cyclic pure dilatational response $\mathbf{D}' = 0$ from a zero-stress state with initial conditions

$$J_{se}(0) = 1, \quad \phi_s(0) = 0.60, \quad \bar{\mathbf{B}}_e(0) = \mathbf{I}. \tag{59}$$

For this case, the total dilatation J from the zero-stress state is specified by

$$J = 1 + 0.1\big[\cos(\pi T) - 1\big], \quad \mathbf{D}\cdot\mathbf{I} = \frac{\dot{J}}{J}, \quad 0 \le T \le 2, \tag{60}$$

where T is a normalized time and J cycles in the range $0.8 \le J \le 1.0$. Since the distortional deformation rate vanishes in this example, the evolution Eq. (28) for ϕ_s reduces to

$$\frac{\dot{\phi}_s}{\phi_s} = \exp\Big[-a_1\Big(\frac{\phi_s}{\phi_J - \phi_s}\Big)\Big]\langle -\mathbf{D}\cdot\mathbf{I}\rangle, \tag{61}$$

which isolates the influence of a_1.

Fig. 1 (a,b) shows the influence of a_1 on the response to pure dilatation. During compression (decrease in J from $J = 1$ to $J = 0.8$) the pressure increases along the curved lines, whereas during expansion (increase in J from $J = 0.8$ to $J = 1$) the pressure decreases to zero along a nearly straight line and remains zero for additional expansion. Also, ϕ_s increases during compression and remains constant during expansion. From this figure it can be seen that as a_1 decreases the initial slope of the pressure curve decreases, the slope of the solid fraction curved increases and the maximum value of the pressure for $J = 0.8$ decreases. This means that the parameter a_1 characterizes the resistance of the granular material to compaction, that is, for small values of a_1 the material compacts rapidly until ϕ_s approaches the jamming value ϕ_J, yielding a smaller elastic dilatation and hence smaller pressure.

For cyclic loading between fixed values of the total dilatation J the first loading causes ϕ_s to attain its maximum value for the amplitude of the cycle. Unloading occurs on the nearly straight line until it vanishes and remains zero during continued expansion. During recompression the pressure remains zero until it intersects the previous unloading curve and then increases following the nearly straight unloading curve. This continues for additional cycles.

From Fig. 1b it can also be seen that the particles are compressible since the volume continues to decrease after the solid fraction ϕ_s approaches its jamming value $\phi_J = 0.64$. This indicates that the particles tend to maintain their spherical shapes with the solid volume fraction remaining nearly constant during compression. However, for highly elastically or inelastically deformable particles it is possible to propose an evolution equation for ϕ_J of the form

$$\dot{\phi}_J = \Gamma_J(1 - \phi_J) \ge 0, \tag{62}$$

where the function $\Gamma_J \ge 0$ requires a constitutive equation. This evolution equation models elastic and inelastic shape changes of the particles and allows the granular material to compact out all porosity with $\phi_J \to 1$. However, this functional form for Γ_J is not used in this paper.

5.2. Steady-state simple shear

For steady-state simple shear with $\mathbf{L}$ given by (43), it follows from (20), (42), (45)–(47) and the evolution Eq. (28) with $a_2 > 0$ that

$$\phi_s = \phi_c, \quad p = \phi_c G_s k_s \frac{\varepsilon_v}{1-\varepsilon_v},$$
$$T_{12} = \mu(I^*)p = \frac{\phi_c G_s}{1-\varepsilon_v}\frac{\gamma_m}{(1+\gamma_m^2)^{1/3}}, \quad L = \frac{I}{d}\sqrt{\frac{G_s k_s \varepsilon_v}{\rho_{sz}}}, \tag{63}$$

where γ_m is determined by (48) and (49).

5.3. Specification of a_c, b_c and calibration of I_0, ε_v based on DEM simulations

The values of ϕ_c, I and $\mu(I^*)$ can be determined by the steady-state simple shear regions in the DEM simulation in [[35], Fig. 1]. With specified values for these quantities (42) can be solved for I_0 to deduce that

$$I_0 = I^*\frac{\mu_2 - \mu(I^*)}{\mu(I^*) - \mu_1}, \quad I^* = I\frac{\phi_J}{\phi_J - \phi_c}. \tag{64}$$

In addition, (26) can be solved for the constant a_c to obtain

$$a_c = \frac{\phi_J}{I^{b_c}}\Big(\frac{\phi_J}{\phi_c} - 1\Big). \tag{65}$$

where μ_1, μ_2 are determined by (25) and the constants in Table 4.

Specifically, to be consistent with the DEM simulation in [[35], Fig. 1]

$$\phi_s = \phi_c = 0.60, \quad I = 0.0003, \quad \mu(I^*) = 0.40. \tag{66}$$

Fig. 2 shows the influence of b_c on the steady-state values of ϕ_c in (26) for a range of I. In the limit that the inertial number approaches zero the critical solid volume fraction ϕ_c approaches the jamming value ϕ_J, with a zero slope at $I = 0$. From this figure it can be seen that the decrease in ϕ_c with increase in I is enhanced by increasing the value of b_c.

For the remainder of the simulations a_c and b_c take the values recorded in Table 4. The values specified in Table 4 are consistent with (66). Also, using the approximation [44] of the stiffness k of the contact springs in the DEM simulations

$$k = \frac{1}{2}\pi d G_s(1+\nu_s), \tag{67}$$

it follows that the steady-state pressure in [[35], Fig. 1] is given by

$$\frac{p\,d}{k} = 9.4\times 10^{-3} = \frac{2p}{\pi G_s(1+\nu_s)}, \quad \frac{p}{G_s} = 9.8437\times 10^{-3}, \tag{68}$$

with the specification $\nu_s = 1/3$. Using the constitutive Eq. (63) for pressure with $\phi_s = 0.6$ this value corresponds to

$$\varepsilon_v = \frac{p}{p + \phi_s G_s k_s} = 6.1147\times 10^{-3}. \tag{69}$$

In this regard, it is noted that this value of elastic compression ε_v was used in all simulations.

5.4. Transient response

This section uses the transient shearing DEM simulations in [35] to calibrate material constants in the proposed model, Specifically, [35] analyzed two types of transient shearing simulations. Both simulations specify the shearing velocity on the boundaries of the shearing region. They start with steady-state simple shear with a negative shearing rate and transition to steady-state simple shear with a positive shearing rate. One simulation maintains simple shearing during the transition. The other simulation maintains constant non-shearing stress components. Material constants are calibrated by matching the results in these simulations.

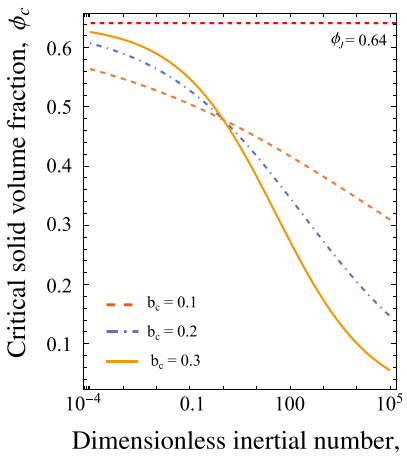

Fig. 2. Influence of the parameter b_c on the critical solid volume fraction ϕ_c (Eq. (26)) that approaches ϕ_J for vanishing inertial number.

To analyze these simulations the velocity gradient $\mathbf{L}$, the deviatoric deformation rate $\mathbf{D}'$ and $\dot{\varepsilon}$ are specified by

$$\mathbf{L} = L\mathbf{e}_1\otimes\mathbf{e}_2 + \frac{1}{3}(\mathbf{D}\cdot\mathbf{I})\mathbf{I} + D'_{11}\mathbf{e}_1\otimes\mathbf{e}_1 - (D'_{11}+D'_{33})\mathbf{e}_2\otimes\mathbf{e}_2 + D'_{33}\mathbf{e}_3\otimes\mathbf{e}_3,$$
$$\mathbf{D}' = D'_{11}\mathbf{e}_1\otimes\mathbf{e}_1 - (D'_{11}+D'_{33})\mathbf{e}_2\otimes\mathbf{e}_2 + D'_{33}\mathbf{e}_3\otimes\mathbf{e}_3 + \frac{L}{2}(\mathbf{e}_1\otimes\mathbf{e}_2 + \mathbf{e}_2\otimes\mathbf{e}_1),$$
$$\dot{\varepsilon} = \frac{1}{\sqrt{3}}\sqrt{4(D'^2_{11} + D'_{11}D'_{33} + D'^2_{33}) + L^2}, \tag{70}$$

where the shearing rate L is specified and the values of $\mathbf{D}\cdot\mathbf{I}, D'_{11}, D'_{33}$, which are active during the transition, need to be determined. Moreover, from (9) and (20) the functional forms of the elastic distortional deformation $\bar{\mathbf{B}}_e$, the pressure p and the deviatoric stress $\mathbf{T}'$, can be specified by

$$\bar{\mathbf{B}}_e = b_{11}\mathbf{e}_1\otimes\mathbf{e}_1 + b_{22}\mathbf{e}_2\otimes\mathbf{e}_2 + b_{33}\mathbf{e}_3\otimes\mathbf{e}_3 + b_{12}(\mathbf{e}_1\otimes\mathbf{e}_2 + \mathbf{e}_2\otimes\mathbf{e}_1), \quad b_{33} = \frac{1}{b_{11}b_{22} - b_{12}^2},$$
$$\bar{\mathbf{B}}'_e = \frac{2b_{11} - b_{22} - b_{33}}{3}\mathbf{e}_1\otimes\mathbf{e}_1 + \frac{-b_{11} + 2b_{22} - b_{33}}{3}\mathbf{e}_2\otimes\mathbf{e}_2 + \frac{-b_{11} - b_{22} + 2b_{33}}{3}\mathbf{e}_3\otimes\mathbf{e}_3 + b_{12}(\mathbf{e}_1\otimes\mathbf{e}_2 + \mathbf{e}_2\mathbf{e}_1),$$
$$|\bar{\mathbf{B}}'_e|^2 = \frac{2}{3}\big(b_{11}^2 + b_{22}^2 + b_{33}^2 - b_{11}b_{22} - b_{11}b_{33} - b_{22}b_{33} + 3b_{12}^2\big),$$
$$p = \phi_s G_s k_s\frac{\varepsilon_v}{1-\varepsilon_v}, \quad \mathbf{T}' = \frac{\phi_s G_s}{1-\varepsilon_v}\bar{\mathbf{B}}'_e, \tag{71}$$

where $b_{ij}, \phi_s, \varepsilon_v$ are determined by the specific problem being solved. Then, the evolution Eqs. (9) require

$$\dot{b}_{11} = \frac{4D''_{11}}{3}b_{11} - \frac{2(D''_{11}+D''_{33})}{3}b_{22} - \frac{2D''_{33}}{3}b_{33} + \frac{4L}{3}b_{12} - \Gamma\Big[b_{11} - \frac{3}{\frac{b_{11}+b_{22}}{b_{11}b_{22}-b_{12}^2} + \frac{1}{b_{33}}}\Big],$$
$$\dot{b}_{22} = -\frac{2D'_{11}}{3}b_{11} - \frac{4(D'_{11}+D'_{33})}{3}b_{22} - \frac{2D'_{33}}{3}b_{33} - \frac{2L}{3}b_{12} - \Gamma\Big[b_{22} - \frac{3}{\frac{b_{11}+b_{22}}{b_{11}b_{22}-b_{12}^2} + \frac{1}{b_{33}}}\Big],$$
$$\dot{b}_{12} = Lb_{22} - (D'_{33} + \Gamma)b_{12}. \tag{72}$$

These results are valid for the transient shearing examples considered in the following sections (see Table 1).

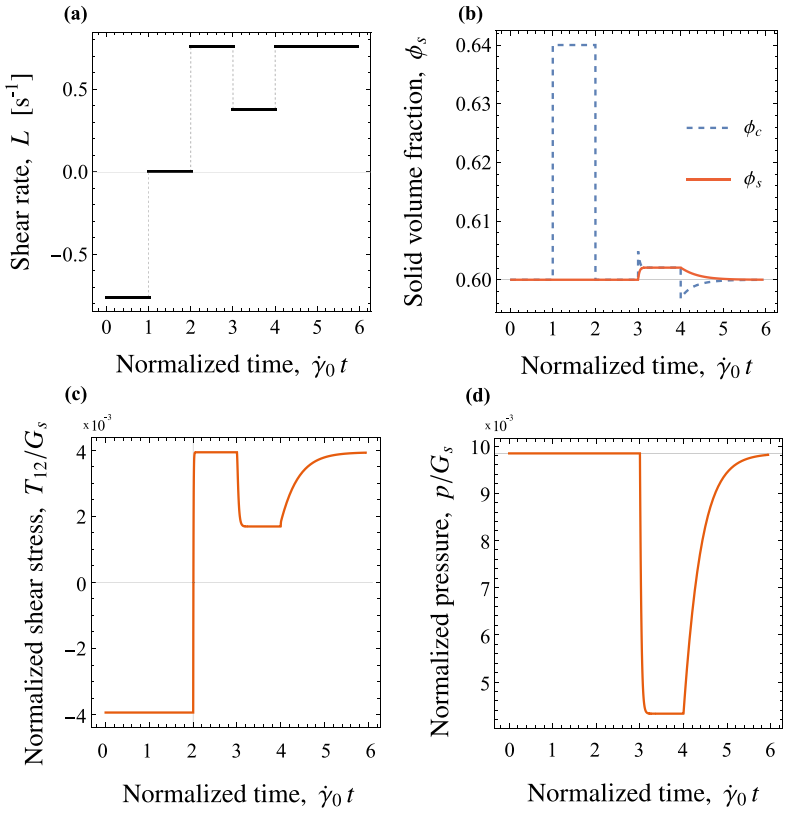

Fig. 3. Simple Shear Jump Test. (a) Shear rate: the initial value of the shearing rate $L(0) = -0.758618$ s^{-1} is consistent with the steady-state simulation in [35]. (b) Solid volume fraction: $\phi_s(0) = 0.60$. When $L = 0$, ϕ_s maintains the steady-state value $\phi_c(0)$, yet ϕ_c abruptly jumps to the jamming value ϕ_J. When L jumps to $\dot{\gamma}_0/2$ from $\dot{\gamma}_0$, ϕ_c reaches a new steady-state value. (c–d) Shear stress and pressure for jump test simulations.

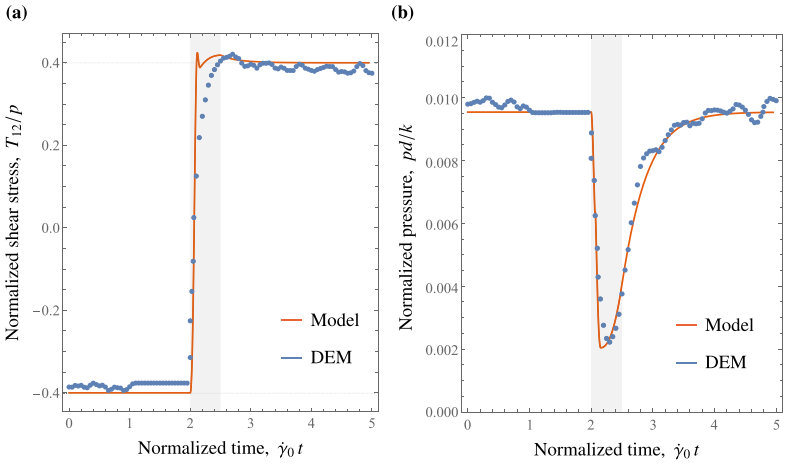

Fig. 4. Transient Simple Shear. Comparison of shear stress (a) and pressure (b) with DEM simulations in ([35], Fig. 1), using a normalized duration $\dot{\gamma}_0 \Delta t = 0.5$ of the transition region where the shear rate increases linearly, indicated with a gray area in the figure.

5.4.1. Transient simple shear (Determination of a_2, a_3 based on DEM simulations)

For transient simple shear at constant volume, the evolution Eqs. (72) are solved with the specifications

$$\mathbf{D} \cdot \mathbf{I} = D'_{11} = D'_{33} = 0. \tag{73}$$

Also, the evolution Eq. (28) is solved for ϕ_s and the value of ε_v is determined by integrating (44) to obtain

$$\varepsilon_v = 1 - \frac{\phi_s(0)}{\phi_s[1 - \varepsilon_v(0)]}, \tag{74}$$

where $\phi_s(0)$ and $\varepsilon_v(0)$ are specified initial values. Specifically, the steady-state initial conditions are specified to be consistent with (66) with I_0 determined by (64) and the initial solid volume fraction is specified

$$\phi_s(0) = 0.6. \tag{75}$$

Also, $\varepsilon_v(0)$ is given by (69), which is used to determine $L(0)$ by (63) and γ by (48) and (49). Then, the initial values of b_{11}, b_{22}, b_{12} are determined by (45).

Since the steady-state value of ϕ_s in (26) depends explicitly on the shearing rate, ϕ_c jumps abruptly when the shearing rate changes. However, the value ϕ_s of the solid fraction, which is determined by the

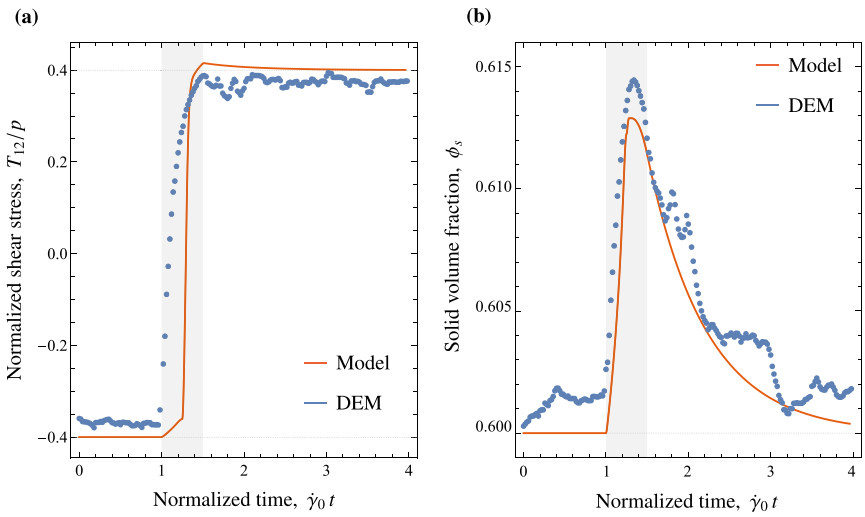

Fig. 5. Transient shear with constant non-shearing components of stress: comparison of shear stress (a) and solid volume fraction (b) with DEM simulations in ([35], Fig. 2), using the same duration of the transition region in Fig. 4.

evolution Eq. (28), exhibits a smoother transition during these changes. Fig. 3 shows the response to a jump test with an initial shearing rate of $L(0) = -\dot{\gamma}_0 < 0$. This value is consistent with the steady-state value of I used for simple shearing in [35] (Fig. 1 therein) and reported in Table 5. The shear rate subsequently jumps to $L = 0$, then to $L = \dot{\gamma}_0$, then to $L = \dot{\gamma}_0/2$, and finally back to $L = \dot{\gamma}_0$. The value $\dot{\gamma}_0$ is kept constant for all figures in this paper. Additionally, the initial values of b_{11}, b_{22}, b_{12} for the steady-state simple shear solution of (72) are recorded in Table 5.

With regard to Fig. 3, it is noted that since $\Gamma = 0$ when $L = 0$, $\phi_s = \phi_c(0)$ remains constant during the period when $L = 0$ even though ϕ_c jumps to the value $\phi_c = \phi_J$. After the jump from $L = 0$ to $L = \dot{\gamma}_0$, $\phi_s = 0.6$ remains constant since $\phi_c = 0.6$ for $L = \pm\dot{\gamma}_0$. During the period when $L = \dot{\gamma}_0/2$ the solid fraction ϕ_s transitions to its new steady-state value of ϕ_c. Finally, after the jump back to $L = \dot{\gamma}_0$, the solid fraction transitions back to the value $\phi_s = 0.6$. This is best observed in Fig. 3b, which compares the responses of ϕ_s and ϕ_c. These results indicate that the steady-state response depends only on the current state of the material and not on the previous history, which is expected for this Eulerian formulation of the constitutive equations. Also, the elastic-viscoplastic response of the proposed model can be seen in the last drop in stress followed by recovery in Fig. 3c and in the pressure in Fig. 3d.

Figure 1 in [35] shows the response of DEM simulations for simple shear with transitions from steady-state with a negative shearing rate $L(0) < -\dot{\gamma}_0$ to zero shearing rate $L = 0$ and then to steady-state with $L = \dot{\gamma}_0$. Figures 1a,b in [35] indicate that when the shearing rate drops to zero the pressure and shear stress remain constant. However, when the shearing rate becomes positive, there is a drop in pressure to about 20% of its steady-state value with a finite transition time followed by an increase in pressure with a longer transition time. Also, the shear stress divided by the pressure increases from its negative steady-state value to its positive steady-state value with a relatively rapid transition time.

The first and second jumps shown in Fig. 3 are qualitatively the same as those in the DEM simulations. However, the response to the jump from $L = 0$ to $L = \dot{\gamma}_0$ is significantly different from that shown in Fig. 1 in [35], which exhibits a transition time during the drop in pressure and a longer transition time to nearly obtain steady-state for $L = \dot{\gamma}_0$. This suggests that during these transition periods the motion of the particles in the DEM simulation is not consistent with the homogeneous deformation rate that is assumed in the formulation of the transient response (70) analyzed here. In the DEM simulations the transient response is obtained by changing the applied velocity of the boundaries which necessarily yields at least some inhomogeneous deformation rate.

To better model the response predicted by the DEM simulation it is assumed that jump in the velocity gradient from $L = -\dot{\gamma}_0$ to $L = 0$ is instantaneous but that the increase from $L = 0$ to $L = \dot{\gamma}_0$ is linear over a transition time determined by the simulations. This is an attempt to model the inhomogeneous shearing rate in the DEM simulation. The pressure presented in ([35], Figure 1) was normalized by the stiffness parameter k so its absolute value (67) is not relevant. Consequently, to compare the pressure predicted by the proposed model with the DEM results, the pressure predicted by the proposed model was scaled linearly to match the initial steady-state value shown in ([35], Fig. 1) and the results are presented in Fig. 4.

The value of the constant a_2, which controls the increase in ϕ_s during the transition, was determined by matching the peak drop in the pressure shown in Fig. 4b. Also, the constant a_3, which controls the rate of decrease in ϕ_s and the transition time $\dot{\gamma}_0 \Delta t = 0.5$ were determined by matching the recovery of the pressure shown in Fig. 4b, that occurs due to elastic expansion of the particles.

5.4.2. *Transient shear with constant non-shearing components of stress (Determination of a_4 based on DEM simulations)*

Figure 2 in [35] shows the response of DEM simulations starting with steady-state simple shear with negative shearing rate $L = -\dot{\gamma}_0$ and transitioning to steady-state simple shear with positive shearing rate $L = \dot{\gamma}_0$ maintaining constant non-shearing components of stress. In contrast with simple shear, this shearing deformation is not isochoric.

Since the diagonal components of stress are constants during the transition it follows that

$$\frac{d}{dt}\Big(\frac{\phi_s \varepsilon_v}{1-\varepsilon_v}\Big) = 0, \quad \frac{d}{dt}\Big[\Big(\frac{\phi_s}{1-\varepsilon_v}\Big)(2b_{11} - b_{22} - b_{33})\Big] = 0,$$
$$\frac{d}{dt}\Big[\Big(\frac{\phi_s}{1-\varepsilon_v}\Big)(-b_{11} + 2b_{22} - b_{33})\Big] = 0, \tag{76}$$

determine the values of $\mathbf{D}\cdot\mathbf{I}$, D'_{11}, D'_{33}. In particular, using (6), (7) and (72) it can be shown that

$$\mathbf{D}\cdot\mathbf{I} = -(1-\varepsilon_v)\frac{\dot{\phi}_s}{\phi_s},$$
$$D'_{11} = \frac{(\mathbf{D}\cdot\mathbf{I} + \Gamma)(b_{11}b_{22} + b_{11}b_{33} - 2b_{22}b_{33}) - 2L(b_{22} + b_{33})b_{12}}{2(b_{11}b_{22} + b_{11}b_{33} + b_{22}b_{33})}, \tag{77}$$
$$D'_{33} = -\frac{(\mathbf{D}\cdot\mathbf{I} + \Gamma)(2b_{11}b_{22} - b_{11}b_{33} - b_{22}b_{33}) - 2Lb_{22}b_{12}}{2(b_{11}b_{22} + b_{11}b_{33} + b_{22}b_{33})}.$$

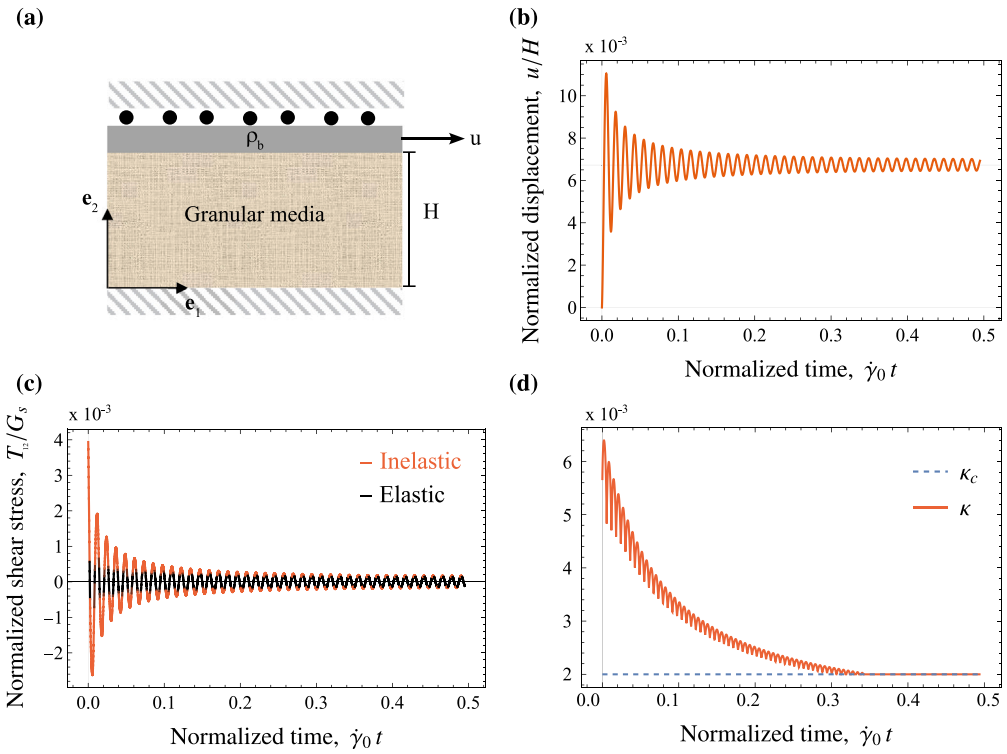

Fig. 6. Response to transition to jamming. (a) Sketch of the model. (b) Time evolution of displacement obtained by solving the governing differential Eq. (82) with the parameters given in (84). (c) Normalized shear stress versus time, with the elastic response regions indicated by the black portion of the curve. (d) Decrease of the hardening variable κ with time until the elastic limit value κ_c is reached.

Also, the value of ε_v can be determined by solving Eq. (71) for the pressure to obtain

$$\varepsilon_v = \frac{p}{p + \phi_s G_s k_s}. \tag{78}$$

In view of (77), the evolution Eq. (28) is rewritten in the forms

$$\frac{\dot{\phi}_s}{\phi_s} = -\Big[\frac{\big(\frac{a_2}{\sqrt{\varepsilon_v}}\big)\langle \phi_s - \phi_c\rangle}{G_s k_s + \big(\frac{a_2}{\sqrt{\varepsilon_v}}\big)\langle \phi_s - \phi_c\rangle\, p}\Big] D_d \qquad \text{for} \quad \phi_s \geq \phi_c,$$
$$\frac{\dot{\phi}_s}{\phi_s} = \frac{a_3 \Gamma \varepsilon_v \langle \phi_c - \phi_s\rangle}{1 - (1-\varepsilon_v)\exp\big[-a_1\big(\frac{\phi_s}{\phi_J - \phi_s}\big)\big] - a_4 \Gamma \varepsilon_v \langle \phi_c - \phi_s\rangle} \qquad \text{for} \quad \phi_c > \phi_s. \tag{79}$$

Now, (23),(24) and (31) are used to deduce that

$$\dot{\varepsilon} = \frac{I}{d\sqrt{3}}\sqrt{\frac{G_s k_s \varepsilon_v}{\rho_{sz}}} \tag{80}$$

which is used with (72) and (77)–(79) to write the rates $\dot{\phi}_s, \dot{b}_{11}, \dot{b}_{22}, \dot{b}_{12}$ as functions of I. Thus, with the help of the expressions for $\dot{\varepsilon}$ in (31) and (80), the value of I is determined by the equation

$$\sqrt{\frac{2}{3}\mathbf{D}' \cdot \mathbf{D}'} = \frac{I}{d\sqrt{3}}\sqrt{\frac{G_s k_s \varepsilon_v}{\rho_{sz}}}. \tag{81}$$

Then, the values of the rates $\dot{\phi}_s, \dot{b}_{11}, \dot{b}_{22}, \dot{b}_{12}$ and the value of I are determined by simultaneously solving the Eqs. (72), (77), (78), (79) and (81) at each step of the integration procedure.

For this example, the initial conditions are those for the steady-state simple shear solution discussed in the previous subsection, which specifies the constant value of p for the simulation with constant non-shearing components of stress. Specifically, using the constants in Table 4 for this simulation, the initial steady-state solution is consistent with p in (68), $\varepsilon_v(0)$ in (69) and the initial values recorded in Table 5.

Fig. 5 shows the response predicted by the proposed model together with results of the DEM simulation in [[35], Fig. 2]. Fig. 5b compares the predictions of the model for ϕ_s with those of the DEM simulation. The value of the constant a_4, which controls the influence of $\mathbf{D}\cdot\mathbf{I}$ on the increase of solid volume fraction ϕ_s during the transition, was selected to closely match the peak value of ϕ_s observed in the DEM simulation (Fig. 5b). To account for the higher initial steady-state value of ϕ_s in the DEM simulation compared to the simulation in ([35], Fig. 1), the value of a_4 was calibrated to result in a slightly lower peak value of ϕ_s. This value of a_4 was necessary to ensure that ϕ_s follows the rapid increase in ϕ_c during the transition onset. Also, the transition time for this simulation was specified by $\dot{\gamma}_0 \Delta t = 0.75$. The results in Figs. 4 and 5 show that the proposed model quantitatively predicts the observations in the DEM simulation in [35].

5.5. The smooth transition to jamming

To study the smooth transition to jamming, consider the transient simple shear problem sketched in Fig. 6a. The granular material of height H is fixed at its bottom surface and its top surface is attached to a block of mass density ρ_b per unit area which can only move horizontally. The system is semi-infinite with a uniform velocity gradient. The equation of motion of the block is given by

$$\rho_b \ddot{u} = -T_{12}, \tag{82}$$

where u is the horizontal displacement of the block in the positive $\mathbf{e}_1$ direction and T_{12} is the shear stress in the granular material. The initial conditions of the system are consistent with the steady-state simple shear solution recorded in Tables 4 and 5 and the initial values of u are specified by

$$u(0) = 0, \quad \dot{u}(0) = \dot{\gamma}_0 H, \tag{83}$$

Also, ρ_b, H and κ_c are specified by

$$\frac{\rho_b}{G_s} = 0.8 \times 10^{-4}\ [\mathrm{s}^2/\mathrm{m}], \quad H = 0.05\ [\mathrm{m}], \quad \kappa_c = 0.002. \tag{84}$$

This value of κ_c is greater than that in Table 5 to increase the elastic limit for low values of pressure.

Figs. 6b-d show the response of the system during the transition to jamming. The displacement plot (Fig. 6b) reveals that the block initially slides and then undergoes oscillations that gradually diminish due to dissipation, eventually transitioning to elastic oscillations as the material jams. The shear stress plot (Fig. 6c) exhibits a similar oscillatory pattern, with the black lines demarcating the elastic response regions. Fig. 6d showcases the corresponding decline in κ until it reaches κ_c, which sets the finite yield value.

6. Conclusions

Constitutive functions in a large deformation continuum model for the response of an elastic–inelastic granular material have been determined using functional forms for $\mu(I)$ rheology and observations based on DEM simulations. The constitutive equations are Eulerian in the sense that they do not depend on arbitrary specifications of a reference or intermediate configuration or a total or plastic deformation measure. The stress in the continuum model is determined by hyperelastic expressions based on a compressible Neo-Hookean strain energy function with the elastic dilatation and the elastic distortional deformation determined by evolution equations. The rate of inelastic deformation in the evolution equation for elastic distortional deformation exhibits a smooth elastic–inelastic transition with the hardening variable calibrated by the rate-dependent steady-state response to simple shear. Also, an evolution equation for the solid fraction is proposed using its steady-state value determined in DEM simulations. Specifically, the non-dissipative response to decrease in the solid fraction at positive pressure is limited by the dissipative response of inelastic distortional deformation to ensure that the total dissipation remains non-negative.

Examples show that jumps in shear rate for transient simple shear cause smooth changes in the state variables and that the steady-state response is truly Eulerian and independent of the history-dependence of loading. Examples are considered which show that the proposed model predicts well results observed in DEM simulations for transient simulations of simple shear and transient shearing with constant non-shearing components of stress. Also, an example has been discussed which shows that the model exhibits a smooth transition from inelastic flowing to elastic oscillations in a jammed state. The model has been developed with three-dimensional equations that can be implemented in computer codes for predicting transient flow of granular materials.

In the analysis outlined in this paper, kinetic energy was deliberately excluded. However, it could be relevant for portraying non-homogeneous deformation observed in inertial transitions or bursts, which can instigate instabilities such as landslides or avalanches [45]. This intriguing subject deserves further exploration as a possible extension of the proposed model.

CRediT authorship contribution statement

M.B. Rubin: Writing – review & editing, Writing – original draft, Supervision, Methodology, Investigation, Formal analysis, Conceptualization. **J. Ciambella:** Writing – review & editing, Visualization, Validation, Software, Investigation, Formal analysis, Data curation. **B. Nadler:** Writing – review & editing, Validation, Supervision, Formal analysis, Data curation.

Declaration of competing interest

The authors declare that they have no known competing financial interests or personal relationships that could have appeared to influence the work reported in this paper.

Data availability

Data was obtained from publicly available sources in the scientific literature.

Acknowledgment

B. Nadler would like to acknowledge the support from the National Science and Engineering Research Council of Canada (NSERC, Grant No. RGPIN- 2018-04573).

References

[1] Jaeger HM, Nagel SR. Physics of the granular state. Science 1992;255(5051):1523–31.
[2] Jaeger HM, Nagel SR, Behringer RP. Granular solids, liquids, and gases. Rev Modern Phys 1996;68(4):1259.
[3] Wang Y, Wang Y, Zhang J. Connecting shear localization with the long-range correlated polarized stress fields in granular materials. Nature Commun 2020;11(1):1–7.
[4] Wang Y, Shang J, Wang Y, Zhang J. Contact force measurements and local anisotropy in ellipses and disks. Phys Rev Res 2021;3(4):043053.
[5] Majmudar TS, Behringer RP. Contact force measurements and stress-induced anisotropy in granular materials. Nature 2005;435(7045):1079–82.
[6] Daniels KE, Kollmer JE, Puckett JG. Photoelastic force measurements in granular materials. Rev Sci Instrum 2017;88(5).
[7] Bi D, Zhang J, Chakraborty B, Behringer RP. Jamming by shear. Nature 2011;480(7377):355–8.
[8] Tian J, Liu E, Jiang L, Jiang Z, Sun Y, Xu R. Influence of particle shape on the microstructure evolution and the mechanical properties of granular materials. C R Mécanique 2018;346(6):460–76.
[9] Blanc L, François B, Delchambre A, Lambert P. Characterization and modeling of granular jamming: models for mechanical design. Granul Matter 2021;23(1):1–13.
[10] Nemat-Nasser S. On behavior of granular materials in simple shear. Soils Found 1980;20(3):59–73.
[11] Subhash G, Nemat-Nasser S, Mehrabadi MM, Shodj HM. Experimental investigation of fabric-stress relations in granular materials. Mech Mater 1991;11(2):87–106.
[12] Goddard JD. Dissipative materials as models of thixotropy and plasticity. J Non-Newton Fluid Mech 1984;14:141–60.
[13] Goddard JD. Continuum modeling of granular assemblies: quasi-static dilatancy and yield. Phys Dry Granular Media 1998;1–24.
[14] Collins IF. Elastic/plastic models for soils and sands. Int J Mech Sci 2005;47(4–5):493–508.
[15] Rollo F, Amorosi A. Isotropic and anisotropic elasto-plastic coupling in clays: a thermodynamic approach. Int J Solids Struct 2022;248(October 2021):111668.
[16] Song C, Wang P, Makse HA. A phase diagram for jammed matter. Nature 2008;453(7195):629–32.
[17] Tong LH, Qi Bowen, Xu Changjie. Fluidity characteristic of granular materials within low frequency dynamics. Int J Mech Sci 2021;202:106508.
[18] Vescovi D, Redaelli I, di Prisco C. Modelling phase transition in granular materials: From discontinuum to continuum. Int J Solids Struct 2020;202:495–510.
[19] Luding S, Jiang Y, Liu M. Un-jamming due to energetic instability: statics to dynamics. Granul. matter, vol. 23, (4):Springer Berlin Heidelberg; 2021, p. 1–41.
[20] Elaskar SA, Godoy LA. Constitutive relations for compressible granular materials using non-Newtonian fluid mechanics. Int J Mech Sci 1998;40(10):1001–18.
[21] Jop P, Forterre Y, Pouliquen O. A constitutive law for dense granular flows. Nature 2006;441(7094):727–30.
[22] Baker JL, Barker T, Gray JMNT. A two-dimensional depth-averaged $\mu(I)$-rheology for dense granular avalanches. J Fluid Mech 2016;787:367–95.
[23] Dunatunga S, Kamrin K. Continuum modelling and simulation of granular flows through their many phases. J Fluid Mech 2015;779:483–513.
[24] Kamrin Ken. Nonlinear elasto-plastic model for dense granular flow. Int J Plast 2010;26(2):167–88.
[25] Tahmasebi P. A state-of-the-art review of experimental and computational studies of granular materials: Properties, advances, challenges, and future directions. Prog Mater Sci 2023;138:101157.
[26] Chialvo S, Sun J, Sundaresan S. Bridging the rheology of granular flows in three regimes. Phys Rev E 2012;85(2):021305.
[27] Trulsson M. Rheology and shear jamming of frictional ellipses. J Fluid Mech 2018;849:718–40.
[28] Majmudar TS, Sperl M, Luding S, Behringer RP. Jamming transition in granular systems. Phys Rev Lett 2007;98(5):058001.
[29] Li Z, Zeng X, Wen T, Zhang Y. Numerical comparison of contact force models in the discrete element method. Aerospace 2022;9(11):737.

[30] Rubin MB. An elastic-viscoplastic model exhibiting continuity of solid and fluid states. Internat J Engrg Sci 1987;25:1175–91.
[31] Hollenstein M, Jabareen M, Rubin MB. Modeling a smooth elastic–inelastic transition with a strongly objective numerical integrator needing no iteration. Comput Mech 2013;52:649–67.
[32] Hollenstein M, Jabareen M, Rubin M B. Erratum to: Modeling a smooth elastic–inelastic transition with a strongly objective numerical integrator needing no iteration. Comput Mech 2015;55:453.
[33] Oda M. Initial fabrics and their relations to mechanical properties of granular material. Soils Found 1972;12(1):17–36.
[34] Nemat-Nasser S. Fabric-stress-deformation relations in granular materials. Tech. rep, California Univ San Diego, La Jolla; 1991.
[35] Sun J, Sundaresan S. A constitutive model with microstructure evolution for flow of rate-independent granular materials. J Fluid Mech 2011;682:590–616.
[36] Eckart C. The thermodynamics of irreversible processes. IV. The theory of elasticity and anelasticity. Phys Rev 1948;73:373–82.
[37] Leonov AI. Nonequilibrium thermodynamics and rheology of viscoelastic polymer media. Rheologica acta 1976;15:85–98.
[38] Rubin MB. Removal of unphysical arbitrariness in constitutive equations for elastically anisotropic nonlinear elastic–viscoplastic solids. Internat J Engrg Sci 2012;53:38–45.
[39] Rubin MB, Einav I. A large deformation breakage model of granular materials including porosity and inelastic distortional deformation rate. Internat J Engrg Sci 2011;49(10):1151–69.
[40] Rubin MB, Attia AV. Calculation of hyperelastic response of finitely deformed elastic-viscoplastic materials. Internat J Numer Methods Engrg 1996;39:309–20.
[41] Rubin MB. Continuum mechanics with Eulerian formulations of constitutive equations. Springer Nature; 2021.
[42] Rubin MB, Vorobiev O Yu, Glenn LA. Mechanical and numerical modeling of a porous elastic–viscoplastic material with tensile failure. Int J Solids Struct 2000;37(13):1841–71.
[43] Rubin MB, Papes O. Advantages of formulating evolution equations for elastic-viscoplastic materials in terms of the velocity gradient instead of the spin tensor. J Mech Mater Struct 2011;6:529–43.
[44] Berzi D, Jenkins JT. Steady shearing flows of deformable, inelastic spheres. Soft Matter 2015;11(24):4799–808.
[45] Clerc A, Wautier A, Bonelli S, Nicot F. Meso-scale signatures of inertial transitions in granular materials. Granul Matter 2021;23(2):1–14.